Supporting information

Chloride Modification of Vacuum-Assisted Blade-Coated Perovskite Solar Cells and Mini-Modules in Ambient Environment

Zikun Cao,[1†] Violeta Elora Gonzalez,[1†] Duong Nguyen Minh,[2] Xinwen Zhang,[2] Yizhao Wang,[3] Kausar Khawaja,[3] Jacob Kjeldahl Jensen,[4] Alex Berzansky,[4] Luisa Whittaker-Brooks,[4] Feng Yan,[3] Joseph M. Luther,[2] He Wang[1,*]

[1] Department of Physics, University of Miami, Coral Gables, FL 33146, USA

[2] National Laboratory of the Rockies, Golden, CO 80401, USA

[3] Materials Science and Engineering Program, School for Engineering of Matter, Transport and Energy, Arizona State University, Tempe, AZ 85287, USA

[4] Department of Chemistry, University of Utah, Salt Lake City, Utah 84112, USA

Email: hewang@miami.edu

[†] These authors contributed equally to this work.

S1. Experimental Methods

S1.1 Materials

All materials were used as received. Formamidinium iodide (FAI), methylammonium chloride (MACl), and phenethylammonium iodide (PEAI) were purchased from GreatCell Solar Materials. Cesium iodide (CsI) was obtained from Alfa Aesar. Lead iodide (PbI_2, 99.99%) and [4-(3,6-Dimethyl-9*H*-carbazol-9-yl)butyl]phosphonic acid (Me-4PACz) were sourced from Tokyo Chemical Industry (TCI). Fluorinated tin oxide (FTO) substrates and lead chloride ($PbCl_2$) were purchased

from Advanced Election Technology. Phenyl-C61-butyric acid methyl ester (PCBM) was purchased from Nano-C. Bathocuproine (BCP), 3-chloropropylamine hydrochloride (Cl-PACl), and all anhydrous solvents were supplied by Millipore Sigma.

S1.2 Perovskite Precursor Preparation

The 1.2 M $FA_{0.92}Cs_{0.08}PbI_3$ perovskite precursor solution was formulated by dissolving FAI (189.9 mg), CsI (24.9 mg), MACl (8 mg), and PbI_2 (553.2 mg) in a mixture of N,N-dimethylformamide (DMF, 885 μL) and N-methyl-2-pyrrolidone (NMP, 115 μL). For additive-modified samples, either 5 mol% Cl-PACl or 2 mol% $PbCl_2$ (relative to Pb) was incorporated into the base precursor. To facilitate the formation of a self-assembled monolayer (SAM) during co-deposition, Me-4PACz was added to the perovskite precursor (0.5 mg/mL) before blade coating for all perovskite films. All preparation steps were conducted within a nitrogen-filled glovebox.

S1.3 Substrate Cleaning and Film Deposition

FTO substrates were rigorously cleaned by scrubbing with a detergent solution, followed by sequential ultrasonication in detergent, deionized water, alcohol, and acetone for 15 minutes each. The substrates were dried with a stream of compressed air and subsequently treated with UV-ozone for 15 minutes immediately prior to use.

Perovskite films were fabricated via a co-deposition blade-coating technique. Approximately 5 μL of the precursor solution was dispensed onto a 2 cm × 2 cm FTO substrate and blade-coated at a speed of 3 mm/s. The wet film was immediately transferred to a vacuum chamber for 2 minutes to induce crystallization, followed by thermal annealing at 150 °C for 10 minutes on a hotplate.

For device completion, a surface passivation layer was applied by spin-coating PEAI solution (1 mg/mL in isopropanol) at 4000 rpm for 30 s, followed by annealing at 100 °C for 5 minutes, in a nitrogen-filled glovebox. The electron transport layer was

subsequently deposited by spin-coating a solution of PCBM (20 mg/mL in chlorobenzene) at 1000 rpm for 30 s, followed by annealing at 90 °C for 5 minutes. A BCP (0.5 mg/mL in isopropanol) interlayer was then spin-coated at 4000 rpm for 30 s, followed by annealing at 80 °C for 5 minutes. Finally, a 90 nm-thick copper electrode was thermally evaporated through a shadow mask to define the active area of 0.105 cm^2.

S1.4 Mini-Module Fabrication

Perovskite mini-modules with an FTO/Me-4PACz+Perovskite/PEAI/PCBM/BCP/Cu structure were fabricated using laser scribing to create series-interconnected sub-cells. The laser patterning process, illustrated in Figure S6, was performed using an 800 nm femtosecond pulsed laser with a home-built motion stage, allowing the substrate to move at a constant speed of 5 mm/s. The process involved four key steps (P1–P4), as detailed below. The P1 step (FTO isolation) was conducted at 80 mW laser power to remove the FTO layer, creating 50 μm-wide isolation lines spaced 6 mm apart. The P2 step (perovskite/ETL removal) was performed at 50 mW; this step selectively ablated the perovskite and electron-transport layers to expose the underlying FTO for the subsequent interconnection, with the P2 line offset 100 μm from the P1 line. The P3 step (back-contact isolation) was executed at 60 mW to remove the metal electrode and underlying layers to electrically isolate adjacent sub-cells, with a 150 μm offset from the P2 line. Finally, the P4 step (peripheral isolation, Figure S6b) involved a final scribe to remove the peripheral device stack down to the glass substrate, preventing edge exposure and ensuring a clean boundary for encapsulation (Figure S6c). The width of the total dead area from the laser scribes was approximately 400 μm, accounting for 6.7% of the total module area. After P4 isolation, the area of each individual sub-cell was defined as 2.04 cm^2.

S1.5 Device Encapsulation

For stability testing, devices were encapsulated using a vacuum lamination process to protect against ambient humidity. A glass cover slide pre-laminated with a thermally activated adhesive film was carefully aligned and placed over the completed device or module. The assembly was then processed in a thermal laminator at 100 °C under a vacuum pressure of 8.6 torr, forming a hermetically sealed structure. A photograph of a resulting encapsulated module is shown in Figure S6c.

S2. Characterization Methods

S2.1 Device Test

Current-density-voltage (J-V) characteristics and steady-state power output were measured using a Keithley 2612B source meter under illumination from a Xenon lamp solar simulator calibrated to AM 1.5G conditions (100 mW/cm^2). Operational photostability was evaluated by maintaining encapsulated devices under continuous one sun (100 mW/cm^2) at open-circuit conditions, at room temperature and 45-55% RH.

S2.2 Film Characterization

Linear absorption spectra were acquired using an Agilent Cary-60 UV-Vis spectrophotometer. Steady-state photoluminescence (PL) measurements were conducted on a Horiba iHR320 spectrometer equipped with a charge-coupled device (CCD) detector, using a 405 nm pulsed laser for excitation. Time-resolved PL decays were recorded via time-correlated single photon counting (TCSPC) on a Horiba DeltaFlex system, employing the same 405 nm excitation source.

X-ray diffraction (XRD) patterns were obtained with a Bruker D8 Advance diffractometer utilizing Cu Kα radiation (λ = 1.5406 Å). The measurements were conducted at 40 kV and 25 mA with a scanning step size of 0.01°. Surface morphology was examined using a FEI Quanta 600F scanning electron microscope (SEM), with

high-resolution images captured on a FEI Nova Nano field-emission SEM operating at an accelerating voltage of 10 keV.

Transient absorption measurements were performed with a commercial pump-probe spectrometer (Helios, Ultrafast Systems). A femtosecond laser system (Coherent Astrella) coupled with an optical parametric amplifier generated the excitation pulses at 400 nm (5 μW power, 5 kHz repetition rate). A broadband white-light continuum served as the probe beam to monitor spectral changes.

X-ray photoelectron spectroscopy (XPS) was performed in a Kratos Axis Supra+ with a dual monochromatic Al/Ag source with high energy resolution.

In-situ transmission measurements of perovskite films during vacuum quenching were carried out by monitoring the transmission of white light through the films. A white light source (peak wavelength ~611 nm) was directed from the top of the vacuum chamber through a glass window, while the transmitted light was collected at the bottom through another glass window using an optical fiber coupled to a visible spectrometer (Ocean Optics). The spectrometer acquired signals every 1 s.

In-situ PL measurements were performed using a Horiba iHR320 spectrometer equipped with a CCD detector. The samples were excited using a 405 nm pulsed laser directed through a glass window into the vacuum chamber. The emission signals were collected with an integration time of 1 s every 2 s.

S3. Data Fitting

S3.1 Time-Resolved Photoluminescence (TRPL) Data Analysis

The TRPL decay curves were fitted using a biexponential decay function: $I(t) = A_0 + B_1 e^{-t/\tau_1} + B_2 e^{-t/\tau_2}$, where A_0 represents the constant background signal. The amplitudes B_1 and B_2 represent the relative contributions of the two decay components.

The average lifetime (τ_{avg}) was calculated using an amplitude-weighted expression: $\tau_{avg} = (B_1\tau_1 + B_2\tau_2) / (B_1 + B_2)$.

Table S1. Fitting parameters for TRPL

	No MACl	MACl	Cl-PACl	$PbCl_2$
τ_1(ns)	37.9	115.4	71.5	111.4
τ_2(ns)	183.6	359.6	251.8	429.9
A_0 (normalized)	-4.2×10^{-6}	1.01×10^{-3}	5.9×10^{-4}	5.09×10^{-3}
$B_1/(B_1+B_2)$ (%)	80.5	76.4	78.5	57.7
$B_2/(B_1+B_2)$ (%)	19.5	23.6	21.5	42.3
τ_{avg}(ns)	66.3	173.1	110.2	246.2

S3.2 Transient Absorption (TA) Data Analysis

The kinetic traces at the ground-state bleaching (GSB) wavelength were analyzed using a triple-component exponential-Gaussian convolution model. In this model, each lifetime component ($\tau_i=1/G_i$) describes a distinct carrier dynamics process, with A_i representing the associated amplitude. The negative amplitude A_1 is attributed to hot-carrier cooling from high-energy states to the band edge. The average lifetime (τ_{avg}) was calculated using an amplitude-weighted expression: $\tau_{avg} = (|A_1|\tau_1 + |A_2|\tau_2 + |A_3|\tau_3) / (|A_1| + |A_2| + |A_3|)$.

Table S2. Fitting parameters for transient absorption spectra

	MACl	Cl-PACl	$PbCl_2$
G_1 (1/ps)	0.066±0.004	0.062±0.003	0.042±0.002
A_1	-0.0031±0.0001	-0.0040±0.0001	-0.0067±0.0001
G_2 (1/ps)	0.0011±0.0001	0.0013±0.0001	0.0011±0.0002
A_2	0.0041±0.0002	0.0044±0.0002	0.0049±0.0005
G_3 (1/ps)	0.000058±0.000007	0.000095±0.000006	0.000054±0.000007
A_3	0.0076±0.0003	0.0075±0.0002	0.0180±0.0006
τ_{avg}	9.1 ns	5.2 ns	11.4 ns

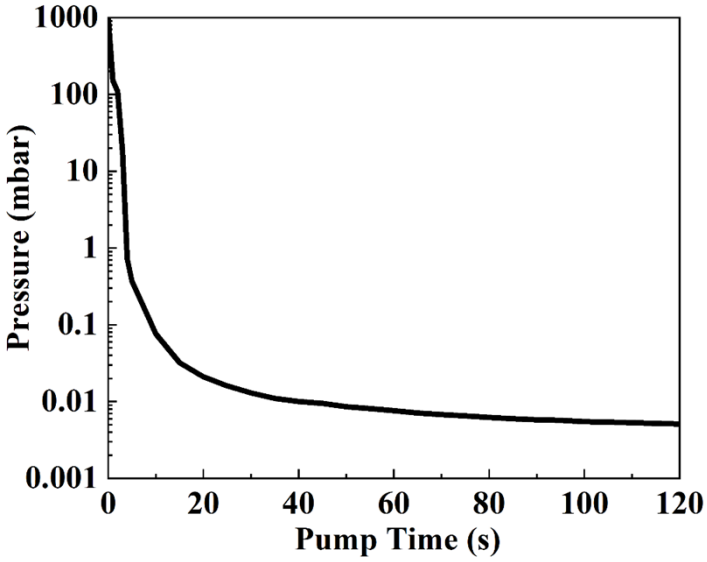

Figure S1. Pressure vs pump time for vacuum chamber.

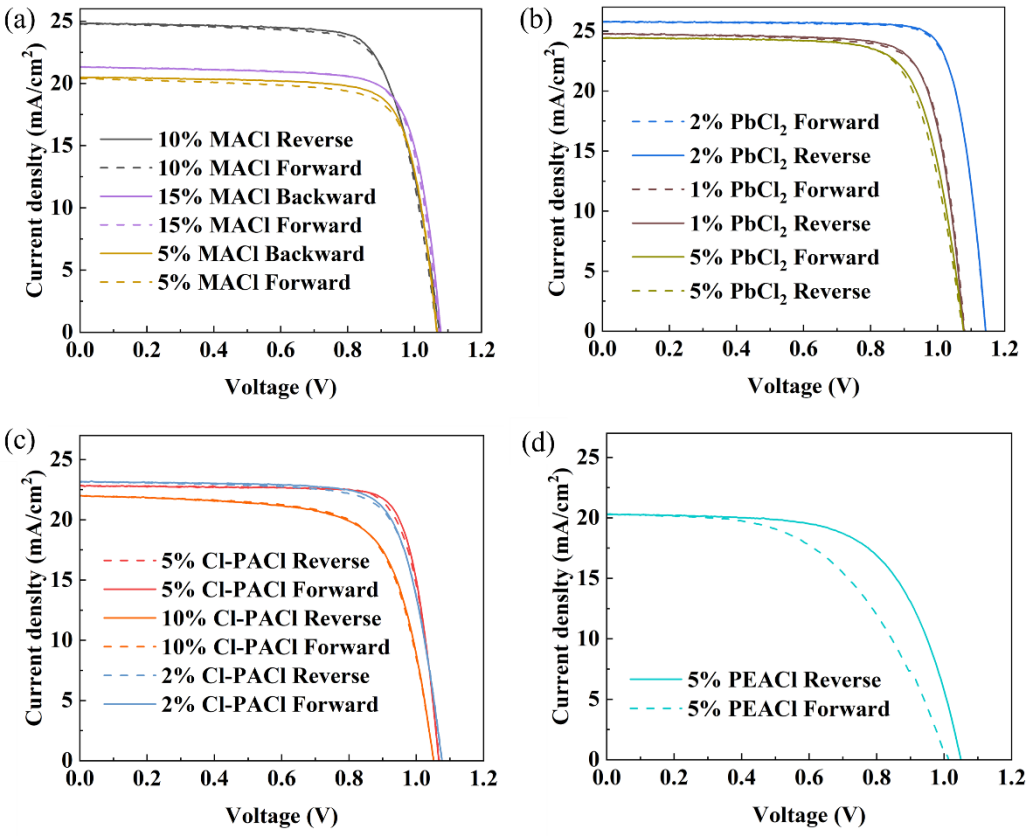

Figure S2. J-V characteristics of perovskite solar cells with different amounts of additives: (a) MACl concentration; (b) $PbCl_2$ concentration; (c) Cl-PACl concentration; (d) 5% PEACl for comparison.

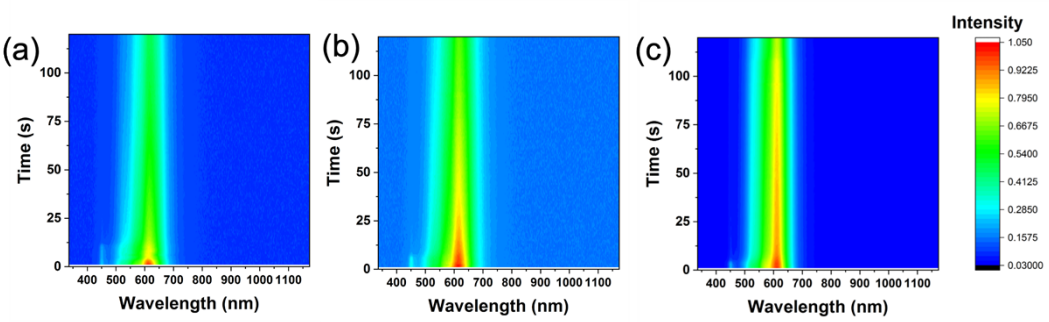

Figure S3. In-situ transmission evolution of perovskite films during vacuum quenching from the liquid precursor to the intermediate phase, including (a) pristine (MACl only), (b) Cl-PACl-, and (c) $PbCl_2$-modified perovskite samples.

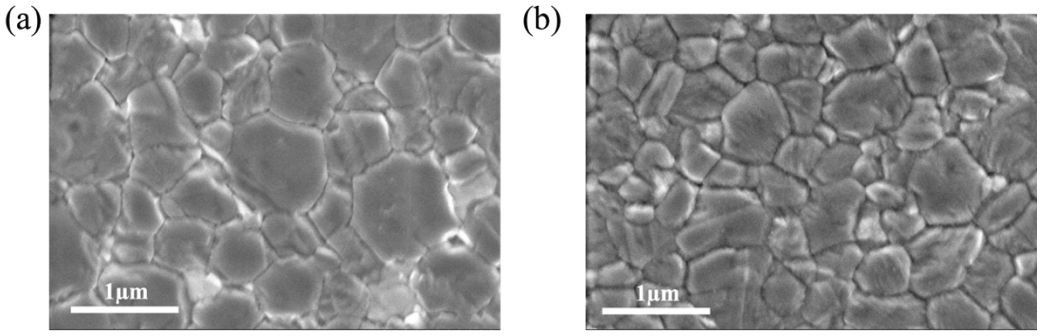

Figure S4. SEM of (a) $PbCl_2$-modified perovskite and (b) PEAI-treated surface passivation.

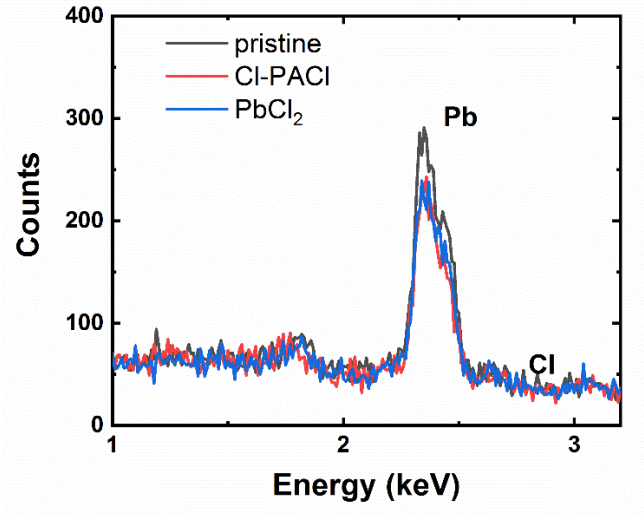

Figure S5. EDS of pristine (MACl only), Cl-PACl-modified, and $PbCl_2$-modified perovskites.

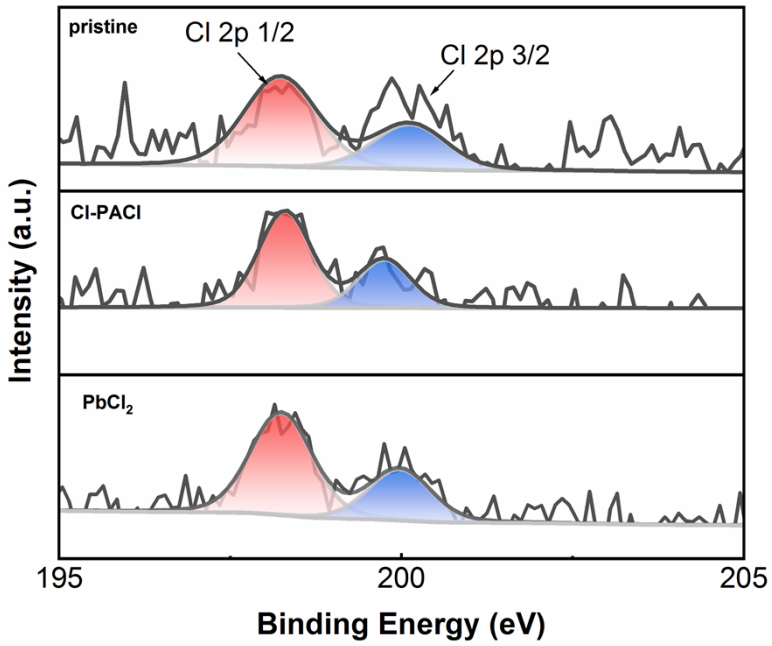

Figure S6. XPS of pristine (MACl only), Cl-PACl-modified, and $PbCl_2$-modified perovskite films.

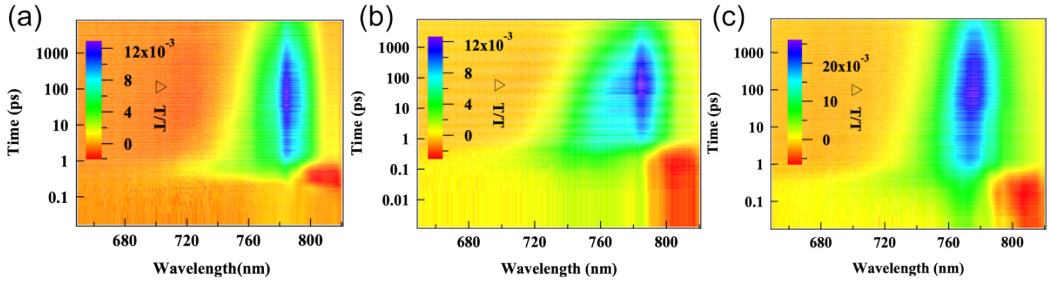

Figure S7. Transient absorption spectra of three different perovskite films: (a) pristine (MACl only), (b) Cl-PACl-modified, and (c) $PbCl_2$-modified perovskite films.

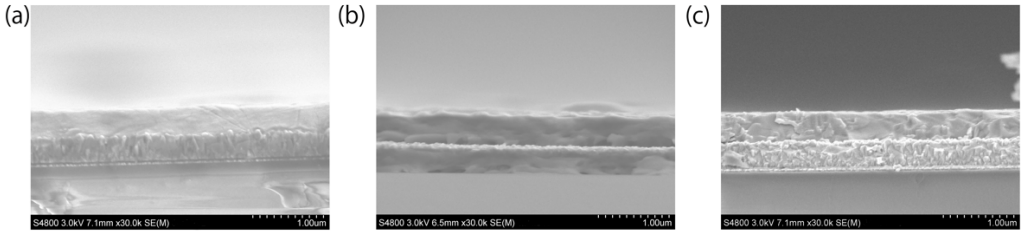

Figure S8. Cross-sectional SEM of three different perovskite films, (a) pristine (MACl only), (b) Cl-PACl-modified, and (c) $PbCl_2$-modified perovskite films.

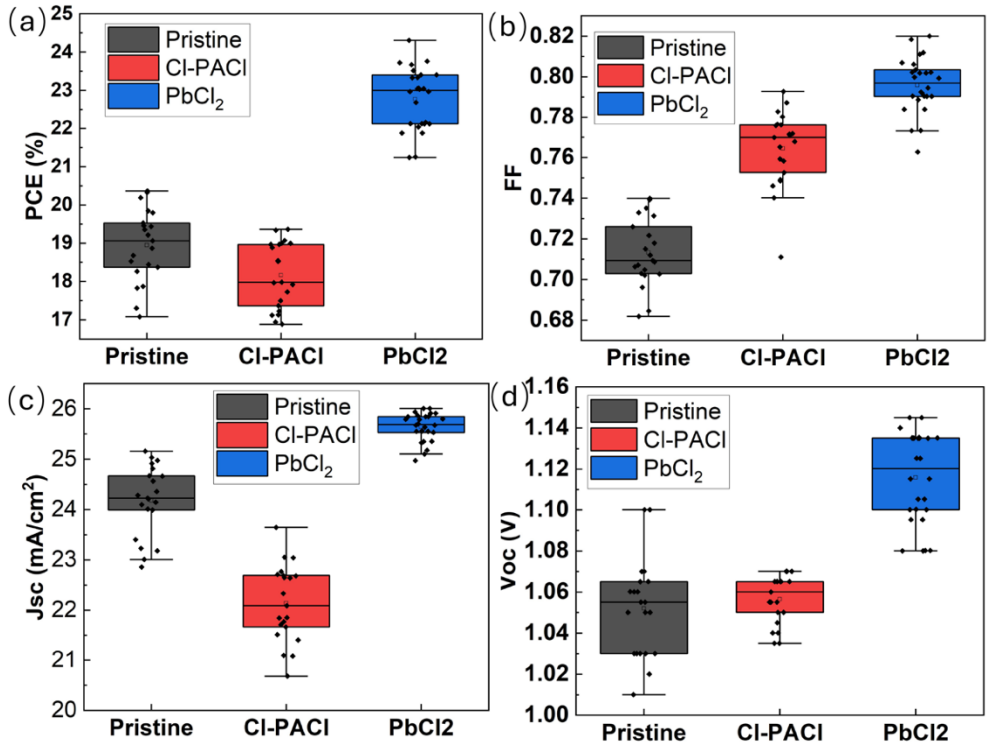

Figure S9. Statistics of solar cells. (a) PCE; (b) FF; (c) Voc; (d) Jsc, with three different perovskite films, pristine (MACl only), Cl-PACl, and $PbCl_2$.

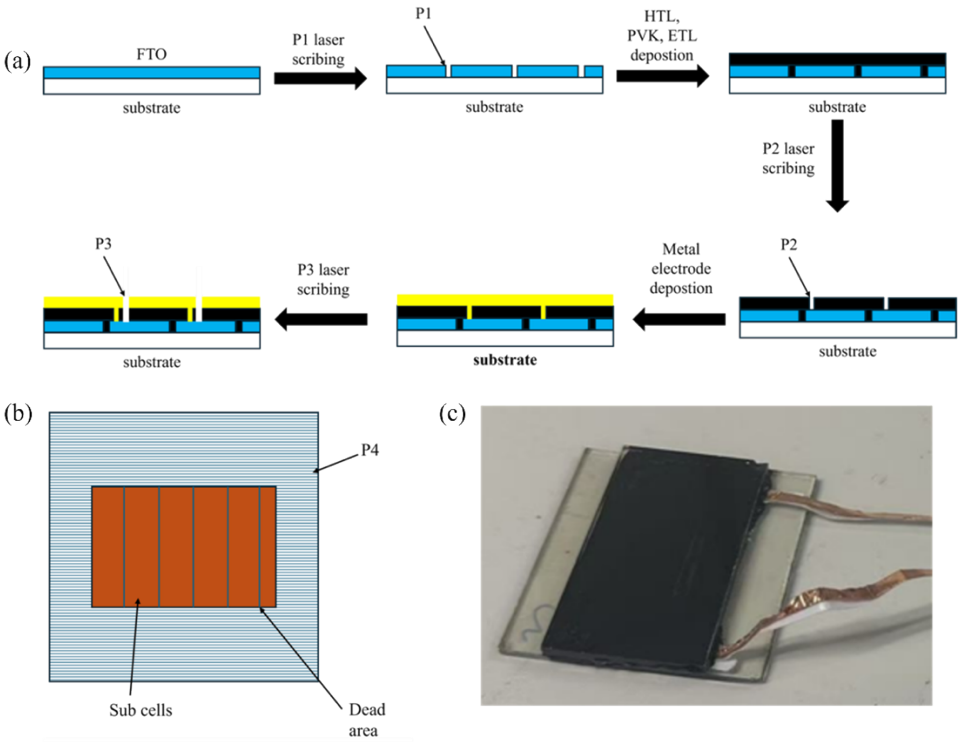

Figure S10. (a) Workflow of fabricating a mini-module. (b) Scheme of mini-module with P4. (c) Photo of encapsulated mini-module.

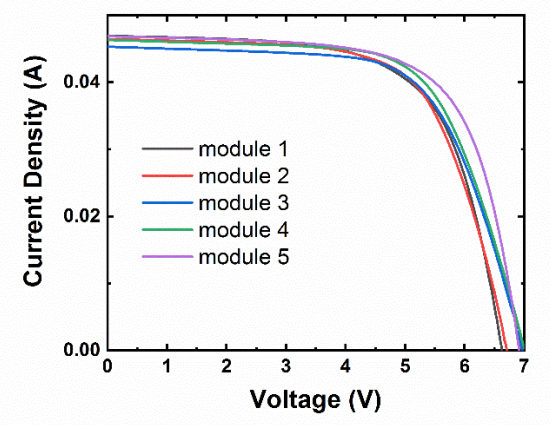

Figure S11. Distribution of PCEs of five independently fabricated perovskite mini-modules based on $PbCl_2$-modified films. The efficiencies of five mini-modules are 16.6%, 16.8%, 16.8%, 17.4%, 18.0%.

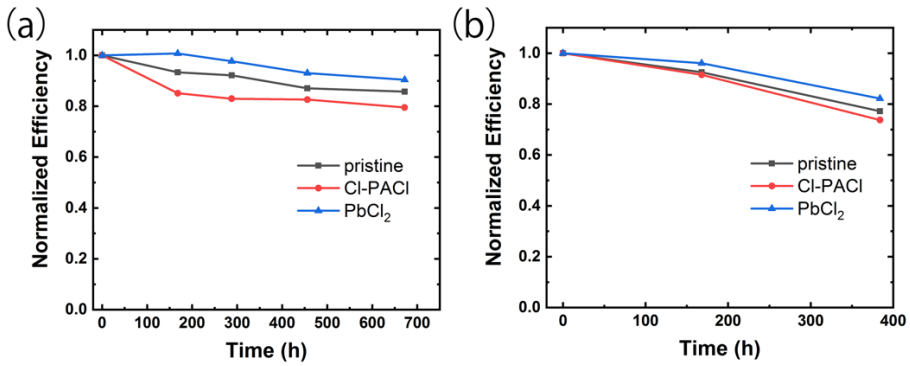

Figure S12. Device stability at different conditions. (a) 65°C in the glovebox for unencapsulated device and (b) 85% RH humidity room temperature for encapsulated device.